Journal of Oceanography, Vol. 60, pp. 893 to 904, 2004

Application of a Two-Way Nested Model to the Seamount Problem

HISASHI HUKUDA[1] and XINYU GUO[2,1]*

[1]*Frontier Research System for Global Change, Showamachi, Kanazawa-ku, Yokohama 236-0001, Japan*
[2]*Center for Marine Environmental Studies, Ehime University, Bunkyo-cho, Matsuyama 790-8577, Japan*

(Received 29 March 2002; in revised form 7 November 2003; accepted 8 December 2003)

A two-way nested model has been constructed and applied to the idealized ocean where a uniform mean flow impinges on the isolated Gaussian-shaped seamount and produces two eddies (cold and warm) in the depths. The performance of the nested model has been evaluated subjectively and objectively. Both subjective and objective analyses confirm the traditional view that the nested model can well capture the performance of isolated eddies. Objective analysis, however, reveals some quantitatively important features of a two-way nested model. One is penetration of improved features into the coarse domain and another is the deterioration of mean flow field inside the nested area, neither of which is clear from subjective analysis. With successful application of two-way nested model to the seamount problem, we expect that such a nested model will also be applicable to other oceanic phenomena, particularly to some coastal problems whose time scale is short and where the topographic effects are dominant.

Keywords:
- Two-way nested model,
- flux-conservation,
- seamount problem,
- eddy behind the seamount,
- objective analysis,
- sigma coordinate model,
- message-passing model.

1. Introduction

The nested model is a useful means to resolve local features that may not be resolved by a coarse grid model alone. The merits of using such a model are clear. One merit is that it gives a tool to resolve a local feature without using a fine grid everywhere, which involves a considerable sacrifice of computer time and memory. Another merit comes from a physical consideration; e.g., more heat is transported by a typhoon to the latitude at which it is found by using a nested model rather than using a coarse grid everywhere.

There are two kinds of nested models. One is a one-way nested model, in which the coarse grid model provides boundary conditions to the embedded fine grid model. The other is a two-way nested model (TNM), in which the fine grid model not only obtains boundary conditions from the coarse grid model, but also feeds its results back to the coarse grid model. Thus, a TNM may be regarded as an attempt to assimilate fine grids into coarse grids with some analogy to a data assimilation model in which data plays the role of the fine grid solution.

In principle, TNM is more reasonable than a one-way nested model. However, in practice, TNM is more difficult to use than a one-way nested model. Compared to its meteorological applications, there are not many examples of two-way nested ocean models. Spall and Holland (1991) developed a TNM and applied it to a barotropic modon and a baroclinic vortex in a flat ocean. Fox and Maskell (1995) extended their methods to an ocean with topography and attempted further refinements of the grid in the vertical direction. The application of their TNM to a front was successful (Fox and Maskell, 1996). It must be noted that all of these TNMs are based on a z-coordinate model. Using on a sigma-coordinate model (Blumberg and Mellor, 1987), Oey and Chen (1992) developed a TNM to simulate meanders and eddies in the Norwegian Coastal Current. Ginis *et al*. (1998) applied the two-way nested scheme for hurricane prediction (Kurihara *et al*., 1979) to a layer ocean model and simulated the response of tropical Pacific Ocean to winds.

The use of TNM to study the coastal waters near or in Japan would be desirable. For example, there are many narrow straits in the Seto Inland Sea that frequently induce topographic eddies with the passage of tidal current. The topographic eddies definitely affect the surrounding wide sea areas (*Nada* in Japanese) but the straits are so narrow that it is unreasonable to completely resolve them in a model including the *Nada*s. The local topography is also important to the Kuroshio. For example, Endoh and Hibiya (2001) have shown that the interaction between the Kuroshio and Koshu Seamount, a

* Corresponding author. E-mail: guoxinyu@dpc.ehime-u.ac.jp

seamount south of Japan, plays a crucial role in deciding the path of Kuroshio.

The above TNMs, except for that of Ginis *et al*. (1998), do not conserve the flux strictly across the nested boundary. Usually a conservative scheme is more complex than a nonconservative one. Furthermore, it is not clear that a conservative scheme can give a better result than a nonconservative one (Spall and Holland, 1991) because in a nested model the coarse grid model cannot resolve the solution of the fine grid model and a conservative scheme enforces the coarse grid fluxes on the fine grid solution and may propagate the erroneous coarse grid field more quickly into the fine grid region (Spall and Holland, 1991).

For relatively short-term integrations, nonconservative boundary conditions are acceptable (Spall and Holland, 1991; Fox and Maskell, 1995). But, as noted by Spall and Holland, this conclusion depends on the model application. The topographic eddies in the Seto Inland Sea are produced by the ambient tidal current. The trapped abyssal anticyclone above Koshu Seamount results from the ambient Kuroshio (Endoh and Hibiya, 2001). These show that the interaction of ambient current with topography is important. Although the eddies reported by Spall and Holland (1991) or the fronts described by Fox and Maskell (1995) could induce a background current, the ambient current itself is not imposed in their models. Therefore, the following question remains to be answered: what is the performance of a TNM with nonconservative boundary conditions in the presence of an ambient current?

In this paper we address such a problem using the TNM that has been constructed based on POM (Mellor, 1998) and PVM (Geist *et al*., 1994). The seamount problem described in Chapman and Haidvogel (1992) and Mellor *et al*. (1998) gives an ideal situation for such a study because it involves both mean flow and isolated eddies for which the validity of the TNM without flux conservation may be examined. Another difference of this study from those of Spall and Holland (1991) and Fox and Maskell (1995) is that we use a sigma coordinate ocean model.

The present paper describes the TNM in Section 2. In Section 3 we revisit the seamount problem and apply our nested model to examine its performance subjectively. In Section 4 we give an objective method to evaluate the error of a nested model. A conclusion is given in Section 5.

2. Description of Model

2.1 Basic ocean model

The basic ocean model we use is a primitive equation model known as POM (Mellor, 1998). This model is briefly outlined as follows. It adopts Arakawa C grids (Arakawa and Lamb, 1977), uses the sigma coordinate as the vertical coordinate (Phillips, 1957) and utilizes the mode split method in which external and internal modes are solved with different time steps (Simons, 1980). It also contains the Mellor-Yamada turbulent closure model and Smagorinsky nonlinear viscosity. Although it is applicable to the orthogonal curvilinear spherical coordinate system, we are only concerned with the rectilinear f-plane system in this study.

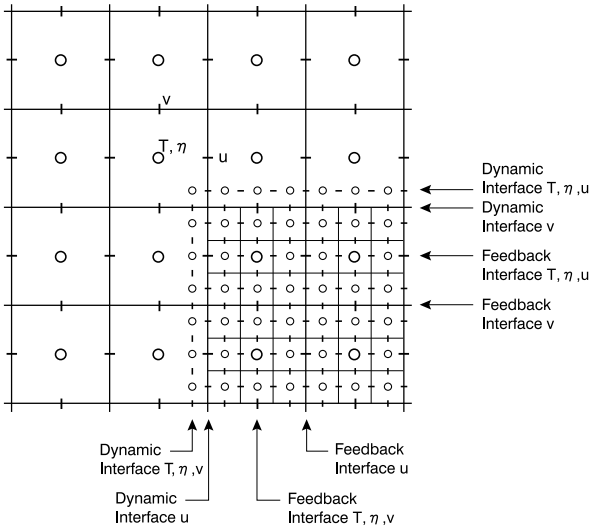

Fig. 1. Nested grid structure: interpolation is done along the dynamic interface. Feedback is made on all grid points within the feedback interface.

2.2 Nesting procedure

In the present nested model, a coarse grid model (CGM) and a nested fine grid model (FGM) are both treated as independent models, except for the communication parts in which two models exchange each variables for interpolation and feedback. Therefore, we actually run two models in parallel. The PVM message-passing model is used for communication. In this model the daemon process called PVMD plays the role of a message-passer. We have observed that latency (i.e. cpu time required for the message-passing process) was quite small (a few percent of the total cpu time) for our Unix workstation. The present model, however, is coded so as to use a minimum CFL time step required by the finest grid model and this is necessary in order to simplify the nesting code. The nested grid structure is depicted in Fig. 1 for a grid ratio of 1:3.

a. Interpolation

The interpolation method used here is based on the idea that the error caused by interpolation may be reduced

by using the values on nearest grids. Thus, the values at the FGM points along the dynamic interface are determined by simple linear interpolation. This is done first along the tangential direction using two adjacent CGM variables to decide the value at the outward grid nearest the dynamic interface (auxiliary point) and then along the normal direction using one CGM variable at the auxiliary point and one FGM variable located inward from the interface by one grid. For the normal velocity, the interpolation in the normal direction is redundant. This operation is written as

$$\phi_i = \varepsilon\Phi_I + (1-\varepsilon)\phi_{i-1} \tag{1}$$

where ϕ_i and ϕ_{i-1} denote an FGM variable at the boundary grid and at the inward grid, respectively, and Φ_I is the value at the auxiliary point that is an intermediate point of the CGM grids outward from the boundary, as interpolated from the adjacent CGM variables along the dynamic interface. Let δx and δX be the grid-width of the fine and coarse mesh, respectively. Referring to Fig. 1, we can set $\varepsilon = 2\delta x/(\delta x + \delta X)$ for the temperature and tangential velocity points, and $\varepsilon = 1$ for the normal velocity points. It is important to note that as POM uses Smagorinsky nonlinear viscosity (A_M), we need to use (1) to determine the value of A_M at the boundary grids of FGM.

b. Feedback

The feedback is incorporated into the model by applying Spall and Holland's (1991) method. In the case of a 1:3 grid ratio (see Fig. 1), this is equivalent to using

$$A_I\Phi_I = \sum_{i=1}^{9} a_i\phi_i. \tag{2}$$

In (2) one coarse grid of area A_I is composed of nine fine grids of area a_i with the constraint that $A_I = \sum_{i=1}^{9} a_i$ (I and i being the CGM and FGM grid point index, respectively). Equation (2) is applied to all CGM prognostic variables within the feedback interface at every time step of external and internal modes.

c. Topography

The topography is handled as follows. First the water depths of FGM and CGM are smoothed using the volume-conserving filter described in Mellor (1998). However, the smoothing is overridden for the CGM depth inside the feedback interface where both the FGM and CGM domain overlap, for which (2) is used to determine the depth. The depths on the FGM boundary grids are interpolated from CGM depths using (1). We should note that this prescription of depth is valid only if the nested boundary is located on a relatively flat depth so that the cross-sectional areas from FGM and CGM are of equal magnitude. For the seamount problem discussed below, we chose the nested boundary to enclose the seamount and the flux error caused by the depth is almost negligible. Thus, since no temporal interpolation error occurs in our TNM which uses the same time step for CGM and FGM, the sole flux error comes from the spatial interpolation error of the model field along the dynamic interface.

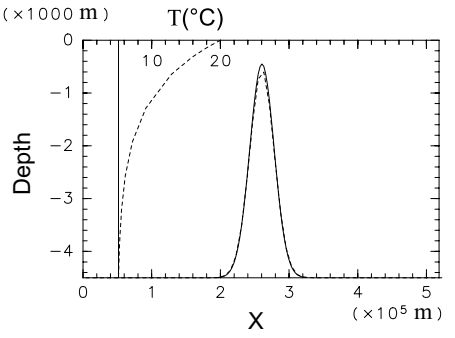

Fig. 2. Seamount model: Solid (dashed) line shows the depth of FGM (CGM). The initial temperature profile of the model is also indicated with a dashed line.

3. Experiments with the Seamount Model

3.1 A seamount model

The seamount model is taken from the default setup in POM. A brief description of the model is given below. The forcing is given by a barotropic mean flow flowing eastward. The ocean, with a size of 500 km × 400 km, is a channel enclosed by rigid walls at the northern and southern boundaries and has an inflow and outflow at western and eastern open boundaries, respectively. We specify a steep seamount with a Gaussian profile

$$h(x,y) = h_\infty\left(1 - \delta\exp\left[-\left\{(x-x_c)^2 + (y-y_c)^2\right\}\Big/ r_a^2\right]\right) \tag{3}$$

where h_∞ = 4500 m, r_a = 25 km and (x_c, y_c) denotes the position of the seamount center. The parameter δ measures the seamount height relative to the oceanic depth and is fixed at $\delta = 0.9$ in this study.

The ocean has an initial stratification in which only temperature varies with the depth z as

$$T = T_a + T_b\exp[\gamma z] \tag{4}$$

where T_a = 5°C, T_b = 15°C and $\gamma = 10^{-3}$ m^{-1} (see Fig. 2). The temperatures at the two open boundaries are determined by upstream differences. Salinity is simply fixed at a constant value (35 psu). Moreover, heat and momentum fluxes at the sea surface are assumed to be zero. Thus,

Table 1. List of experiments: the figures in parentheses refer to CGM to FGM values in order and (δT_e, δT_i) refer to the external and internal mode time step.

No.	Grid type	Grid spacing (km)	Grid number ($I \times J$)	CFL time (δT_e, δT_i sec)	Case
1	SGM low	8.1	65×49	(9, 270)	SGM-l
2	SGM high	2.7	195×147	(3, 90)	SGM-h
3	Doubly nested	(8.1, 2.7)	(65×49, 50×38)	(3, 90)	A_3^2
		(8.1, 0.9)	(65×49, 146×110)	(1, 30)	A_9^2
4	Triply nested	(8.1, 2.7, 0.9)	(65×49, 50×38, 38×38)	(1, 30)	A_3^3
5	Movable nest	(8.1, 2.7, 2.7)	(65×49, 38×38, 38×38)	(3, 90)	AIs
		(8.1, 2.7, 2.7)	(65×49, 50×50, 50×50)	(3, 90)	AIm
		(8.1, 2.7, 2.7)	(65×49, 62×62, 62×62)	(3, 90)	AIl

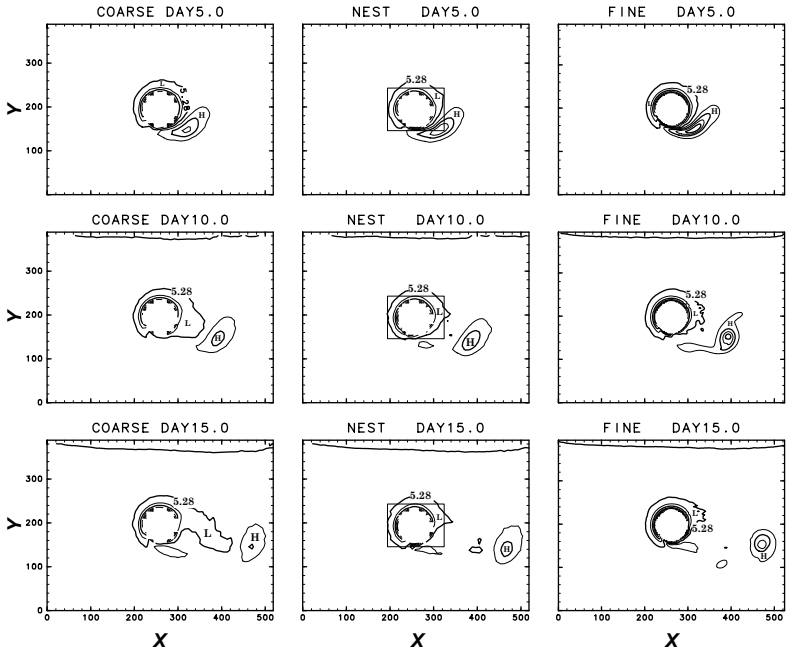

Fig. 3. Temperature contours at 4000 m of Case SGM-l (left), Case A_3^2 (middle), and Case SGM-h (right). Contours are drawn at every 0.024°C.

the only forcing is the uniform eastward flow that impinges on the seamount. The boundary conditions at eastern and western ends are taken from the default setup in the POM's subroutine BCOND. Both CGM and FGM start from the same initial conditions with zero elevation, uniform eastward flow of 0.2 ms^{-1}, and the temperature specified in (4).

Huppert and Bryan (1976) and Chapman and Haidvogel (1992) have described the solution of the above seamount problem in detail. Basically, we obtain a similar solution. As soon as the model starts, two eddies with opposite signs of vorticity are formed at the seamount. The upwelling on the upstream side of the seamount compresses water columns and induces an anti-cyclonic (cold) eddy. The downwelling on the downstream side stretches water columns and induces a cyclonic (warm) eddy. These two eddies co-rotate clockwise around the seamount. While radiating inertia gravity waves, two eddies interact and reach geostrophic balance after a couple of days. After Day 2~3 the advective process becomes dominant. The warm cyclonic eddy is detached from the southeastern foot of the seamount and the mean flow advects it to the east. Meanwhile, the cold anti-cyclonic eddy remains trapped around the seamount.

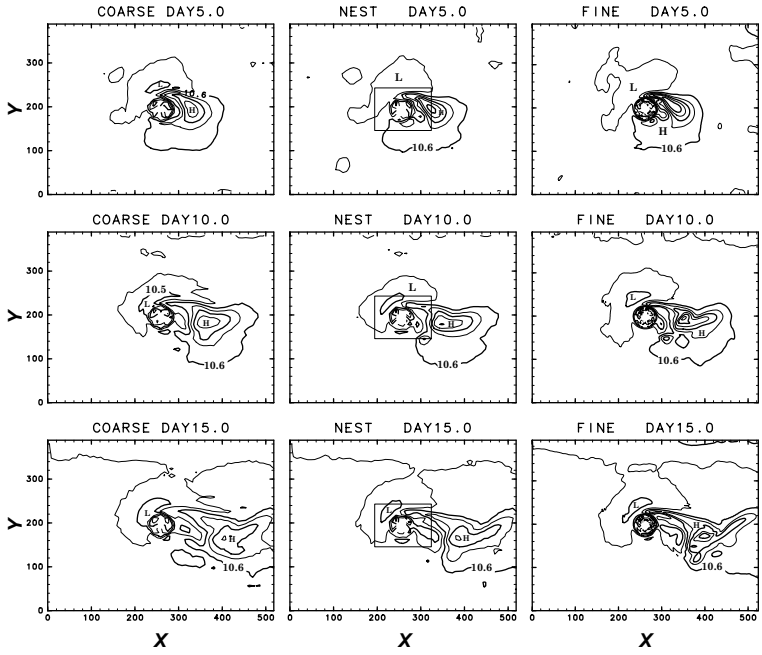

Fig. 4. As Fig. 3, but for temperature at 1000 m. Contours are drawn at every 0.05°C.

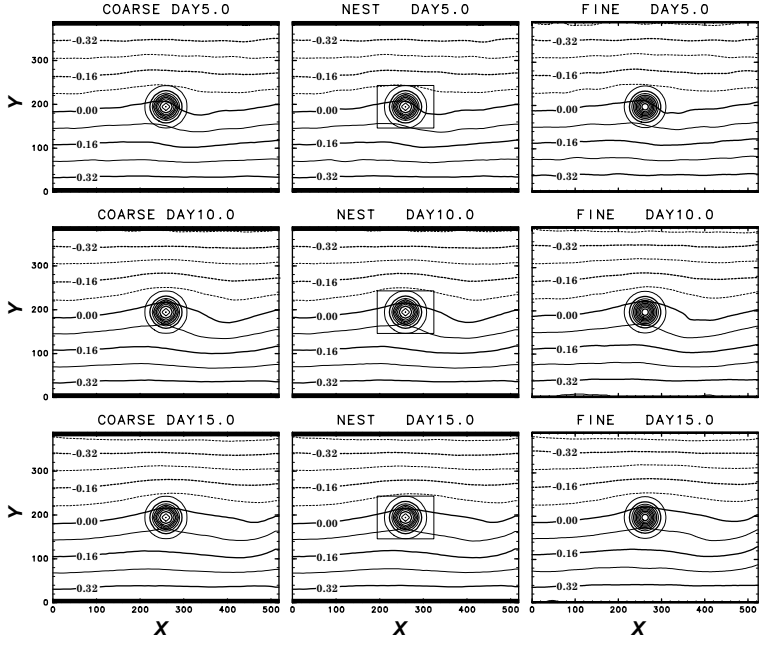

Fig. 5. As Fig. 3, but for elevation. Contours are drawn at every 0.08 m. Seamount topography is also shown.

3.2 Experiments with the nested model

Table 1 summarizes the experiments conducted in this study. Two control experiments (Exp. 1, 2) with two single grid models (SGM), each having a low resolution (8.1 km) or a high resolution (2.7 km) everywhere, were run prior to the nested model experiments. All models use the same eleven σ levels given by σ = 0, –.018, –.036, –.071, –.143, –.286, –.429, –.571, –.714, –.857, –1 and the same horizontal momentum and heat diffusion parameters, HORCON = 0.2 and TPRNI = 1 (see

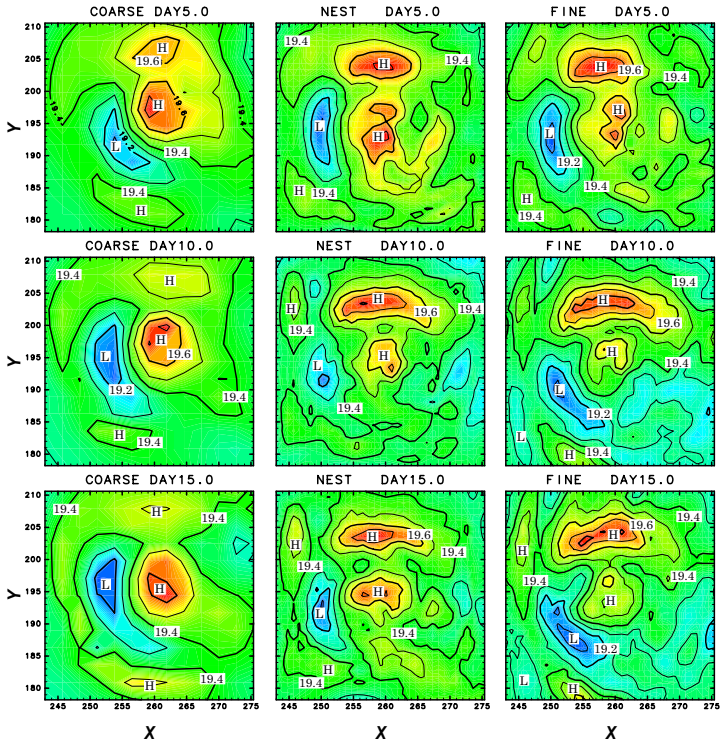

Fig. 6. Temperature contours at 50 m of Case A_3^2 (left), Case A_3^3 (middle), and Case A_9^2 (right). Contours are drawn at every 0.1°C

Mellor (1998) for definition). The nested model was run stably for a month. However, because the flow reaches a nearly steady state after 15 days, the period for which the warm eddy generated at the seamount flows out of the eastern end, only results until Day 15 are presented below.

In the remainder of this section we describe two kinds of experiments using the TNM; the first one only uses a nested area fixed over the seamount (Case A) while the second covers each of cold and warm eddies by using multiple nests (Case AI). We compare the performance of our nested model with that of two SGM results.

a. Case A

The doubly nested model where the nested boundary is located on a flat bottom surrounding the seamount is standard and will be referred to as Case A_3^2 (hereafter, a subscript refers to the grid ratio and a superscript refers to the degree of nest). Since the two eddies have a strong vertical structure with bottom intensification (Chapman and Haidvogel, 1992), we first show the evolution of temperature contours at 4000 m depth (Fig. 3), where the TNM result (labeled nest) is compared with two SGM results (labeled coarse and fine). We can see how the horizontal grid size affects the eddy evolution. The cold eddy surrounding the seamount is more diffusive on the coarse grid, but less diffusive on the fine one. The nested model can resolve this feature well. On the other hand, the warm eddy flowing away from the seamount is much weaker on the coarse grid, but is enhanced on the fine grid. The nested model clearly fails to reproduce this feature simply because the resolution is not enough there. The horizontal resolution also affects the evolution of the warm eddy in such a way that the eddy structure is much more self-organized in the high-resolution model result.

Fairly speaking, Case A_3^2 seems to show a reasonable result and confirms our previous knowledge of TNM: a mesoscale feature inside the nest can be resolved reasonably well, but other features outside the nest are only poorly resolved; thus, as expected, it yields a hybrid result of CGM and FGM characteristics. Case A_3^2, however, clearly fails in reproducing the warm eddy structure as calculated by the high-resolution model. This failure prompted us to use multiple nests so as to cover each of the eddies generated around the seamount. Before doing so, however, we want to look at the model performance at shallower depths.

How well does the same nested model perform at the shallow level? Figure 4 shows the evolution of temperature contours at 1000 m depth on the coarse, nested and fine grids. The nested model result is taken from the same outputs as in Case A_3^2. We see that little noise appears across the nested boundary and its performance compares well with that at the deep level.

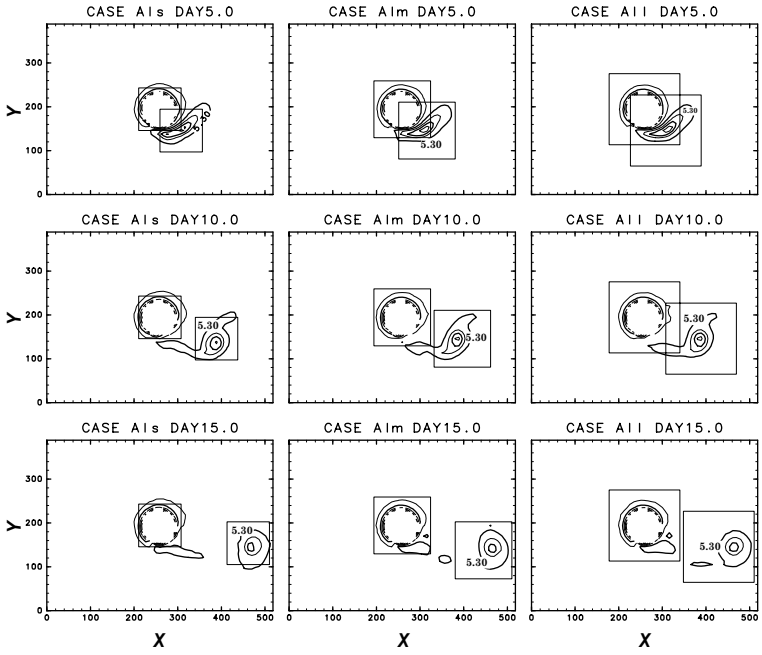

Fig. 7. Temperature contours in Case AI. Contours are drawn at every 0.025°C. Nest size increases in order from left (Case AIs), middle (Case AIm) to right (Case AII).

The final comparison in Case A_3^2 is made for the elevation and is shown in Fig. 5. The northward decline of sea level implies the presence of an eastward flow, which is disturbed by the seamount topography. The sea level of a nested model (middle) compares well with that of a high-resolution model (right), although the difference among three (coarse, nest and fine) models seems to be small. Thus, subjective judgment of the nested model performance for the mean flow field is less critical than that for the eddy field.

A triply nested model, which is a simple extension of the doubly nested model, may be used to resolve a fine structure near the surface. This case amounts to setting one more nest in Case A_3^2 and will be referred to as Case A_3^3. For this high-resolution grid, the control experiment that uses a SGM with a grid spacing of 0.9 km is not feasible. Instead, we decided to compare this result with that of the doubly nested model with a high grid ratio of 1:9 (Case A_9^2). This is permissible because, with a high grid ratio, the doubly nested model is less subject to the influence from the nested boundary, so it will be regarded as an approximate control experiment for the innermost area of the triply nested model.

Figure 6 compares temperature contours at 50 m-depth between the triply nested model (middle) and two doubly nested models, one with a high grid ratio of 1:9 (right) and other with a low grid ratio of 1:3 (left). We see that the eddy at the seamount summit becomes finer as resolution increases from 2.7 km (left) to 0.9 km (middle and right). We also see that both high-resolution models reproduce a similar pattern, but the triply nested model (middle) is more susceptible to the boundary effect compared to the doubly nested model (right), as mentioned above.

The dominant stationary eddies appear at the seamount summit and may be recognized as the Taylor caps described by Chapman and Haidvogel (1992). According to their experiments, the Taylor caps remain trapped around the seamount only at low Rossby numbers. With a speed of $u = 0.2$ ms^{-1}, the present case gives Ro = 0.08 and satisfies Chapman and Haidvogel's (1992) criterion for Taylor caps to be trapped near the seamount summit. Thus, Fig. 6 seems to give further credit to the TNM performance.

b. Case AI

Since the warm eddy moves downstream as time passes, it is necessary to introduce a movable fine mesh to follow and resolve the warm eddy. The movable mesh was incorporated in the present model by following the method of Kurihara *et al.* (1979). We refer the reader to that paper for details of the movable mesh technique. The only thing to mention here is to replace (1) by

$$\phi_i = \Phi_0 + \left(\frac{\partial \Phi_0}{\partial X}\right)(x_i - X_0) + \left(\frac{\partial \Phi_0}{\partial Y}\right)(y_i - Y_0) \qquad (5)$$

where (x_i, y_i) and (X_0, Y_0) are the coordinates of the fine

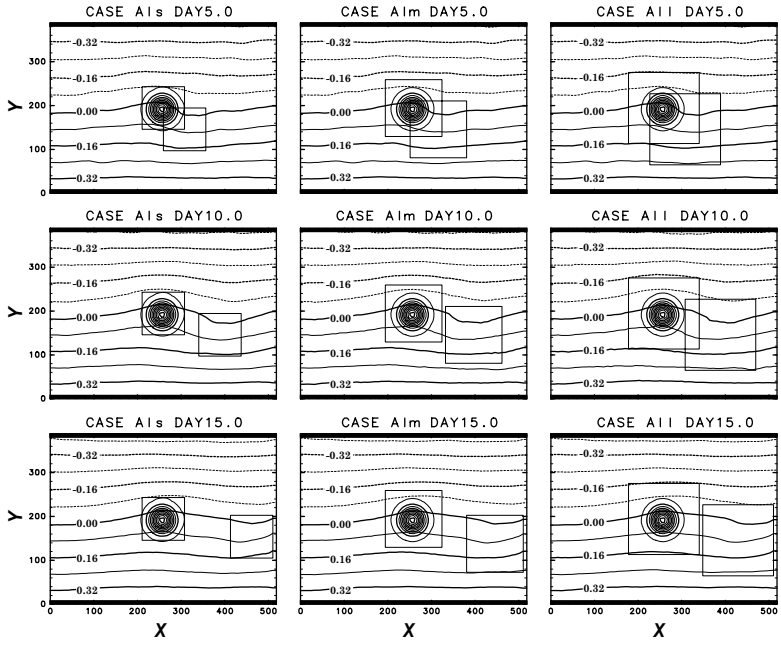

Fig. 8. As Fig. 7, but for elevation. Contours are drawn at every 0.08 m. Seamount topography is also shown.

and coarse grids in the area that was newly created when the mesh moved. The apparent characteristic of (5) is that adding (5) for ϕ_i over one coarse grid leads to the value at the CGM grid (Φ_0) so that a conservation law holds during the mesh movement.

Initially two nested areas are placed to cover each eddy and the nest covering the warm eddy is allowed to move with the eddy. Figure 7 shows three cases simulated by the multiply nested model for which the nest size was increased slightly from Case AIs to Case AII. Generally speaking, Case AIs seems to give enough size to reproduce two eddies well. The similarity of Case AIs to the high-resolution SGM in Fig. 3 is remarkable: the detached warm eddy structure is well reproduced in this model. It also appears that as the nest size increases, the resolved eddy field becomes closer to the high-resolution result.

Figure 8 compares the elevation field in Case AI. Subjectively, we can see little noise in the sea level that could be caused by the presence of two nested fine mesh areas. There remains, however, a question of how the flux error affected the performance of our TNM when the nested area is placed in the mean flow field. We evaluate these errors as well as the errors in Case A in the next section. Because the experimental results have so far been interpreted only according to a subjective judgment of the simulation results, it is not certain that the judgment is free from personal bias. The evaluation of the model performance by objective analysis makes this point clear.

4. Objective Analyses

4.1 Subjective versus objective

In the previous section we judged the nested model performance based on a visual comparison of the resolved features with those of the SGM. Such a *subjective* judgment certainly gives us a base to verify whether the nested model performed well. It is, however, more desirable to seek another way in which the model performance can be *objectively* evaluated. This may be more convincing than asking the reader to compare wiggles in figures.

We consider two methods to evaluate the model performance quantitatively. These are the conventional methods used to see the accuracy of TNM: one in which the geometric quantities of eddies are estimated and the other in which the root mean square (RMS) errors of the field variables are estimated.

4.2 Estimate of eddy properties

Figure 9 compares the area occupied by the cold eddy ($T < 5.28$°C) among the coarse, fine and nested model as in Case $A_3{}^2$ at 4000 m. We can clearly see the similarity of the curves between the fine and nested model and the dissimilarity of these to the curve of the coarse model. Furthermore, we see that the nested curve lies between the coarse and fine model curves, fitting between them. Figure 9 thus quantitatively reconfirms our subjective remarks on the nested model performance.

Figure 10 compares the maximum temperature of the

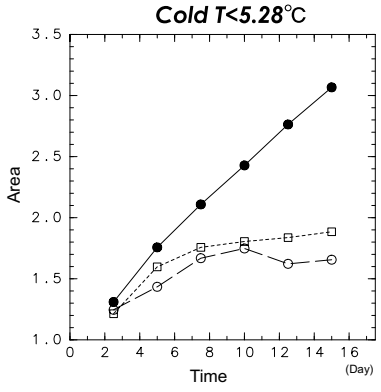

Fig. 9. Time evolution of the cold eddy area with $T < 5.28$°C at 4000 m in Case SGM-l (solid circles), Case $A_3{}^2$ (open squares), and Case SGM-h (open circles). Area is made non-dimensional by dividing by the seamount area at 4000 m.

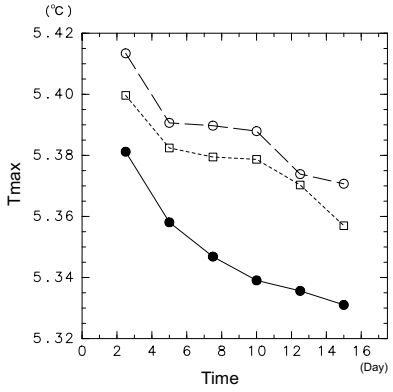

Fig. 10. Time evolution of the warm eddy's maximum temperature in Case SGM-l (solid circles), Case AIs (open squares), and Case SGM-h (open circles).

warm eddy among the coarse, fine and the movable nested model as in Case AIs. The curves of the fine and nested model are very close while the coarse model gives much smaller maximum values. Again, the nested curve fits between the coarse and fine model curves and reconfirms our subjective remarks.

These objective analyses clearly show that the eddy properties associated with the temperature field are well predicted by the TNM. This success is likely due to the isolated feature seen in the temperature contours at 4000 m-depth as TNM has a good capacity to resolve such an isolated phenomenon.

However, Fig. 11 shows some counterproductive performance of the TNM where the predicted track of the warm eddy center is less satisfactory than that of the coarse model. In their study of typhoon simulation, Ley and Elsberry (1976) showed that the track of Typhoon

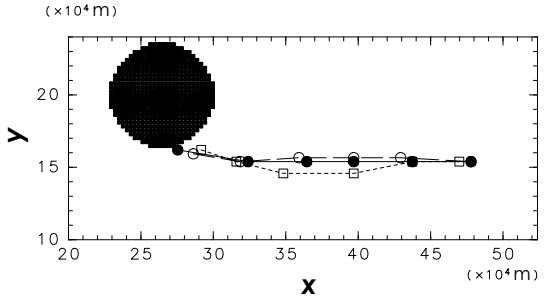

Fig. 11. Trajectories of the warm eddy center in Case SGM-l (solid circles), Case AIs (open squares), and Case SGM-h (open circles).

Irma is closer to the coarse model result than to the nested model one. It is interesting to see the similarity between their study and the present one, although the two studies treat very different subjects. The reason for this deterioration is likely due to the change in a mean flow that affects the movement of an isolated eddy. We examine this conjecture in the next subsection.

4.3 Estimate of root mean square errors

The reason why the mean flow is changed by the use of TNM is interesting. To estimate the change quantitatively, we must devise a measure of error in the mean flow and the eddy field. For this purpose we introduce the root mean square (RMS) error of the nested model variable relative to the true solution that is given approximately by the fine model result. To see the effect of feedback from FGM to CGM, we calculate RMS errors separately for the inside and outside region of a nested area. Let us denote these errors as ε_i and ε_o, respectively. Thus, we define

$$\varepsilon_i = \sqrt{\frac{\sum\left(\Phi_n - \Phi_f\right)^2}{N_i}} \Bigg/ \sqrt{\frac{\sum\left(\Phi_c - \Phi_f\right)^2}{N_i}} \qquad (6)$$

$$\varepsilon_o = \sqrt{\frac{\sum\left(\Phi_n - \Phi_f\right)^2}{N_o}} \Bigg/ \sqrt{\frac{\sum\left(\Phi_c - \Phi_f\right)^2}{N_o}} \qquad (7)$$

where Φ_n, Φ_f, Φ_c are the quantities of the nested, fine and coarse grid model, respectively; N_i and N_o are the numbers of the grid points on the inside and outside of the nest, respectively; the sum in (6) and (7) is taken over the CGM grid points lying inside and outside the nest, respectively. As the value of the FGM variable, we used a nine-point averaged value of Φ_f defined on the CGM grid.

Note that the RMS error of the nested model is nor-

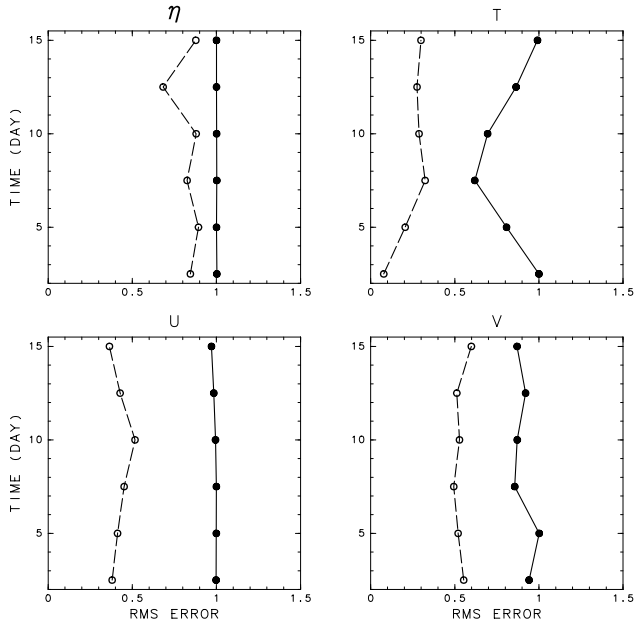

Fig. 12. Root mean square errors at 4000 m for Case A_3^2 plotted against time for regions of inside (open circles) and outside (solid circles) of the nested area.

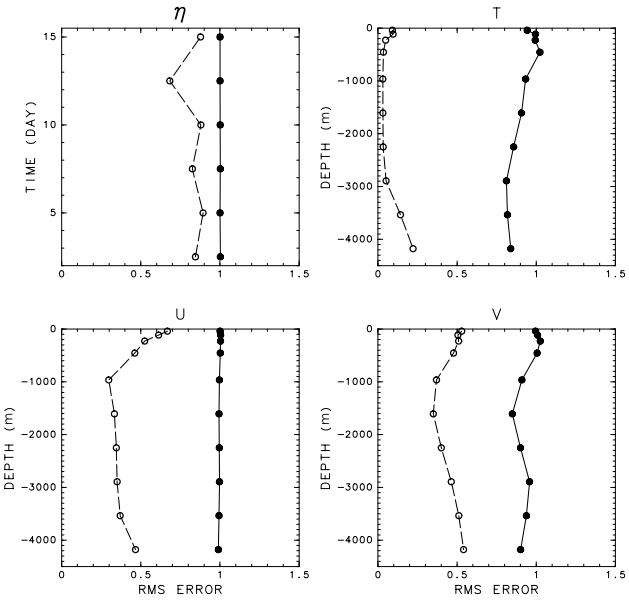

Fig. 13. As Fig. 12, but plotted against depth except for the elevation.

malized with that of the coarse model. Thus if ε_i, $\varepsilon_o < 1$, the nested model performance improves on the coarse model, while if ε_i, $\varepsilon_o > 1$, the nested model performance is inferior to the coarse model. The RMS errors were calculated for elevation (η), temperature (T), and zonal and meridional velocity components (U, V) using (6) and (7).

a. Case A

We first look at the RMS errors in Case A_3^2. Figure 12 shows these errors at 4000 m plotted against time at the interval of 2.5 days. We see that all errors inside the nest (marked by open circles) are less than unity for this short-time evolution, implying that the TNM improved on the coarse model. An interesting feature in Fig. 12 is that the temperature error outside the nest also decreases from unity for periods between Day 2.5 and Day 15, which means that the improvement of temperature inside the nest affected the temperature outside the nest and reduced the error there. This is a merit of having a TNM where the outside CGM solution is influenced by the nested FGM solution. Another feature to be noticed in Fig. 12 is that the sea level error inside the nest (<0.9) is less improved compared with the temperature error in the same region (<0.3). This is caused by the error associated with interpolation of the elevation, which increases due to the sea level gradient along the nested boundary associated with a mean flow field.

To make the above interpretation more concrete, we calculated the RMS errors that show vertical profiles averaged over whole time periods (Fig. 13). We see that a greater improvement is attained for temperature (<0.2) than elevation (<0.9). The velocity errors are of intermediate values (<0.8) between them, but closer to the elevation error. This is because the mean flow is barotropic and the sea level gradient is a main component in determining the flow.

b. Case AI

It is of interest to extend the above analysis to the movable nest case. Figure 14 shows the RMS errors for Case AIs. Because this case uses two nests, one fixed and the other movable, two kinds of RMS errors are introduced for each eddy. In this case the elevation error increased from unity, implying that the TNM performance deteriorates below the coarse model. However, the temperature error still remains smaller than unity and improves on the coarse model. Generally, the temperature error inside the movable nest is larger than that inside the fixed nest.

In Fig. 15 the RMS errors averaged over the whole periods are plotted against the depth. We see that near-surface zonal velocity (U) errors for the warm eddy become large, but decrease as depth increases. This error may be explained by the pressure gradient error associated with the large elevation error and by the fact that the eddy traced by the movable mesh is at 4000 m and not near the surface. The three-dimensional eddy structure generated behind the seamount is thus quite difficult to follow by a simple two-dimensional nesting technique.

The reason for the deterioration of sea level in this case is attributable to two causes. One is the increase of flux error in Case AIs as the nested area doubled from

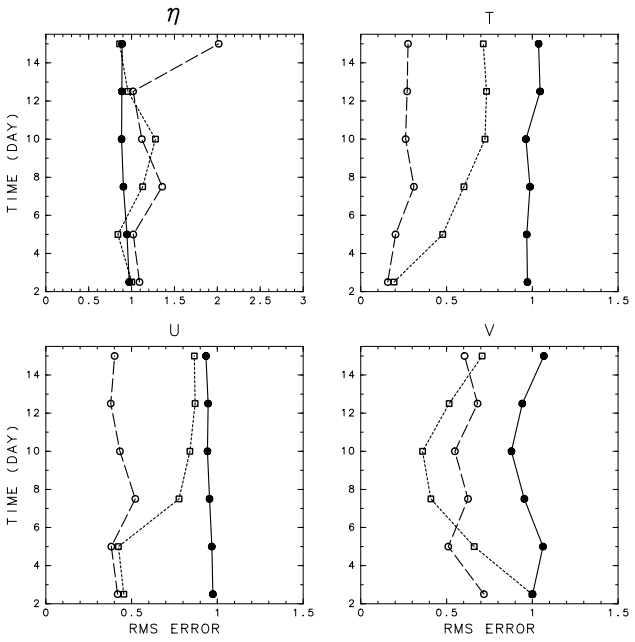

Fig. 14. Root mean square errors at 4000 m for Case AIs plotted against time for regions of nested cold eddy area (open circles), nested warm eddy area (open squares), and outside of the nested areas (solid circles).

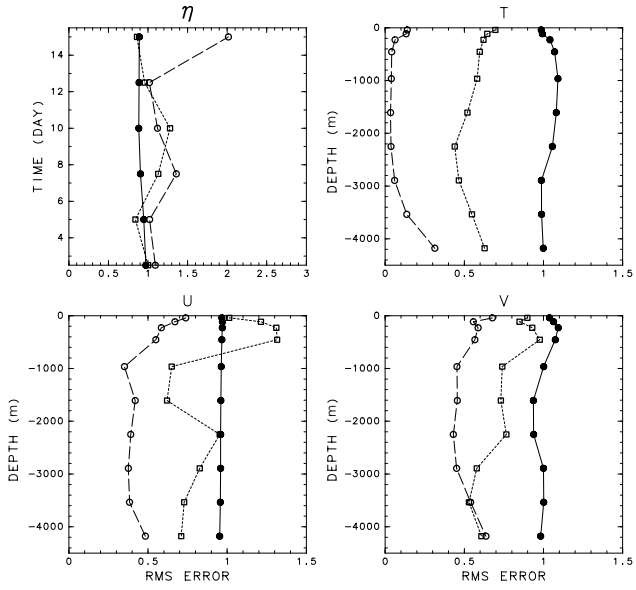

Fig. 15. As Fig. 14, but plotted against depth except for the elevation.

Case A. Because the flux error is proportional to the size of a nested area for the TNM without flux conservation, we expect larger flux errors in Case AIs than Case A, as well as in Case AII rather than Case AIs. The resulting change in a mean flow, as shown in Fig. 11, leads to the larger RMS error than the coarse model by changing the location of the warm eddy. It is not likely that the mesh movement over the seamount affects the flux error because the seamount topography is perfectly covered with two fine nests. Thus, we can say that the presence of a mean flow field, by geostrophy, generates the large gradient of sea level along the nested boundary and favors large interpolation errors.

Table 2. RMS errors for the warm eddy averaged for time.

	Case AIs	Case AIm	Case AII
η	1.011	1.047	1.289
T at 4000 m	0.574	0.373	0.294

Table 3. RMS errors for the cold eddy averaged for time.

	Case AIs	Case AIm	Case AII
η	1.27	1.217	1.292
T at 4000 m	0.246	0.197	0.232

Further calculations of RMS errors in Case AIs to Case AII show that as the size of the nested area increases, the temperature error decreases whereas the elevation error increases for the warm eddy (see Table 2). This is because the warm eddy structure is well isolated in the current problem and the TNM usually improves such a local feature with increasing nest size. The sea level contours, on the other hand, are not localized in the present case and have a wide coverage, straddling the whole nest, so the increase of the nest size will increase the error.

A similar trend of RMS errors is seen when we compare Case AIs to Case AII for the cold eddy (Table 3), but the values this time show a less definite trend than that of the warm eddy.

5. Conclusion

By constructing a TNM that does not have the flux-conserving property and applying it to the idealized seamount problem, we have studies the applicability of such a nested model to the case when an ambient current produces isolated eddies. The nested model was run for a short time of 15 days and its performance has been evaluated using both subjective and objective analyses. Subjective analysis is not new as it reviews our knowledge of the TNM that is well applicable to the mesoscale, isolated patterns. Objective analysis using the root mean square error was then introduced to estimate the error of a nested model both inside and outside of the nest. This analysis gives us two new features. One is a penetration

of the improved features from fine to coarse grid areas. Another is deterioration of the sea level error associated with the mean flow field relative to the temperature error of the eddy field, which is not clear at all from the subjective analysis only. Therefore, with the objective analysis method proposed in this study, one may attain deeper insight into the problems related to the nested model.

The present study apparently shows both the merit and demerit of the two-way nested model without flux conservation. The model has proved to be useful for simulating the isolated feature of an eddy field observed in the seamount problem. However, its performance is not very much improved for simulation of the mean flow field because our model does not conserve the fluxes across the nested boundary, in common with most past models. The presence of mean flow produces, by geostrophy, the large gradient of sea level along the nested boundary and this leads to the interpolation error of flux. This error in turn changes the mean flow field and thus affects the eddy position advected by that mean flow.

This kind of error might be more serious when we treat a more general situation characterized by a steep continental slope and baroclinic western boundary currents like the Kuroshio. Then we must choose the nested area carefully in order to circumvent the large gradient of the scalar variables such as depth, temperature and sea level, which may increase the interpolation error. Accordingly, the size and position of the nested area may not be chosen from economic point of view only, so as to eliminate the flux error as completely as possible. However, the TNM must be a useful tool to study the tide-induced topographic eddies in the Seto Inland Sea because most of the straits there are surrounded by relatively flat *Nada*s and the eddies have a short lifespan.

Acknowledgements

This work was done as part of the Japan Coastal Ocean Predictability Experiment (JCOPE) project, supported by Japan Marine Science and Technology Center. We thank Dr. Takashi Kagimoto and Dr. Jim Kohl for advises and supports in computational aspects, and Ms. Tomoe Mikami for drawing figures. Comments of two reviewers were helpful in improving the manuscript.

References

Arakawa, A. and V. R. Lamb (1977): Computational design of the basic dynamical processes of the UCLA general circulation model. p. 174–265. In *Methods in Computational Physics*, **17**, ed. by J. Chang, Academic Press.

Blumberg, A. F. and G. L. Mellor (1987): A description of a three-dimensional coastal ocean circulation model. p. 1–16. In *Three-Dimensional Coastal Ocean Models*, ed. by N. Heaps, Amer. Geophys. Union.

Chapman, D. C. and D. B. Haidvogel (1992): Formation of Taylor caps over a tall isolated seamount in a stratified ocean. *Geophys. Astrophys. Fluid Dyn.*, **64**, 31–65.

Endoh, T. and T. Hibiya (2001): Numerical simulation of the transient response of the Kuroshio leading to the large meander formation south of Japan. *J. Geophys. Res.*, **106**, 26833–26850.

Fox, A. D. and S. J. Maskell (1995): Two-way interactive nesting of primitive equation ocean models with topography. *J. Phys. Oceanogr.*, **25**, 2977–2996.

Fox, A. D. and S. J. Maskell (1996): A nested primitive equation model of the Iceland-Faeroe front. *J. Geophys. Res.*, **101**, 18259–18278.

Geist, A., A. Beguelin, J. Dongarra, W. Jiang, R. Manchek and V. Sunderam (1994): *PVM: Parallel Virtual Machine—A User's Guide and Tutorial for Networked Parallel Computing*. MIT Press, England.

Ginis, I., R. A. Richardson and L. M. Rothstein (1998): Design of a multiply primitive equation ocean model. *Mon. Wea. Rev.*, **126**, 1054–1079.

Huppert, H. E. and K. Bryan (1976): Topographically generated eddies. *Deep-Sea Res.*, **23**, 655–679.

Kurihara, Y., G. J. Tripoli and M. A. Bender (1979): Design of a movable nested-mesh primitive equation model. *Mon. Wea. Rev.*, **107**, 239–249.

Ley, G. W. and R. L. Elsberry (1976): Forecasts of Typhoon Irma using a nested -grid model. *Mon. Wea. Rev.*, **104**, 1154–1161.

Mellor, G. L. (1998): User's guide for a three-dimensional, primitive equation, numerical ocean model. Princeton University, 35 pp.

Mellor, G. L., L. Y. Oey and T. Ezer (1998): Sigma coordinate pressure gradient errors and the seamount problem. *J. Atmos. Oceanic Technol.*, **15**, 1122–1131.

Oey, L. Y. and P. Chen (1992): A nested grid ocean model with application to the simulation of meanders and eddies in the Norwegian Coastal Current. *J. Geophys. Res.*, **97**, 20063–20086.

Phillips, N. A. (1957): A coordinate system having some special advantages for numerical forecasting. *J. Meteor.*, **14**, 184–185.

Simons, T. J. (1980): *Circulation Models of Lakes and Inland Seas*. Can. Bull. Fish. Aquat. SCI. 203, 146 pp.

Spall, M. A. and W. R. Holland (1991): A nested primitive equation model for oceanic applications. *J. Phys. Oceanogr.*, **21**, 205–220.